CHAPTER

The nonlinear processes in active monitoring 3.4

Marat S. Khairetdinov and Gyulnara M. Shimanskaya
Institute of Computational Mathematics and Mathematical Geophysics SB RAS, Novosibirsk, Russia

Chapter Outline

3.4.1 Introduction

The purpose of active vibroseismic monitoring of seismically dangerous zones is to observe the rheological characteristics of the geological medium during the geodynamic processes that precede large earthquakes. Such monitoring is based on regular sounding of the Earth using recurrent seismic oscillations from low-frequency vibrators. Each sounding is a vibrosession, an analysis of the medium's response parameters extracted from the recorded data (Alekseev et al., 2004, 1998). The repeatability of vibrosessions can be disrupted by various interfering factors: seasonal factors associated with the freezing and thawing of the ground under the vibrator, instrumental errors affecting the intensity characteristics of the radiation field, etc. There is thus a difficulty of providing informative field parameters independent from these unwanted factors.

In addition, vibrosessions are accompanied by nonlinear effects that manifest themselves during the radiation and propagation of vibroseismic oscillations. The

Active Geophysical Monitoring. DOI: https://doi.org/10.1016/B978-0-08-102684-7.00011-X

problem with nonlinear effects occurring during acoustic wave propagation in elastic isotropic media has been studied for several decades. In particular, Polyakova (1964) investigated those nonlinear effects that appear in an elastic isotropic medium during finite deformations and the propagation of an elastic wave through calculation of cubic terms in the elastic energy. Polyakova showed that the interaction between longitudinal and transverse waves leads to the appearance of second harmonics in the transverse wave. More recently, Korneev et al. (1998) presented results based on Murnaghan's elastic theory for elastic wave propagation in isotropic solids, as well as a summary of the major results from the nonlinear interaction of plane elastic waves. Other important studies involving the nonlinear effects of wave propagation in an elastic, isotropic medium are presented in the works of Zarembo and Krasilnikov (1966), Rudenko and Soluyan (1975), and Brekhovskich and Goncharov (1982).

Nikolaev (1987) suggests that fractured media in seismically active regions cause nonlinear effects in propagating waves. The related problems have not only scientific value, but also have practical implications, related to the sensitivity and accuracy of vibroseismic monitoring. This chapter describes some experiments aimed at estimating the nonlinear effects caused by vibrators, as well as the propagation of seismic waves over a 335 km long region of the earth's crust during periods of lunar—solar tides.

We show that taking into account the amplitude ratios between the multiple and fundamental harmonics of seismic wave fields enables monitoring results to be independent of seasonal and instrumental variations. At the same time, the high sensitivity of these ratios to small stress variations in the Earth's crust is retained.

3.4.2 Nonlinear phenomena

Nonlinearity in seismic wave propagation is caused in two ways: by the source and by the geological medium. Source nonlinearity results from source—ground coupling and from the strong nonlinear properties of the soil under the source, leading to generation of sub- and multiple harmonics. As an illustration, Fig. 3.4.1 presents the spectrum versus time oscillations radiated by four types of vibrators: the centrifugal vibrator CV-100 (Fig. 3.4.1A) with an initiation force of 100 t, the hydroresonance vibrator HRV-50 (Fig. 3.4.1B) with an initiation force of 50 t, the centrifugal vibrator CV-40 (Fig. 3.4.1C) with an initiation force of 40 t, and the hydraulic vibrator HV-10/100 (Fig. 3.4.1D) with an initiation force of 10 t (Glinsky et al., 2002). For the vibrator CV-100, the generated spectrum is associated with a linear frequency modulation (sweep signal) of 6.25—9.5 Hz and duration of 600 seconds, for the vibrator HRV-50: 5—7 Hz and 1400 seconds, and for hydraulic vibrator HV-10/100, respectively, 10—60 Hz and 60 seconds. In all cases, the nonlinear radiation effect is characterized by the appearance of second and third harmonics in the spectra.

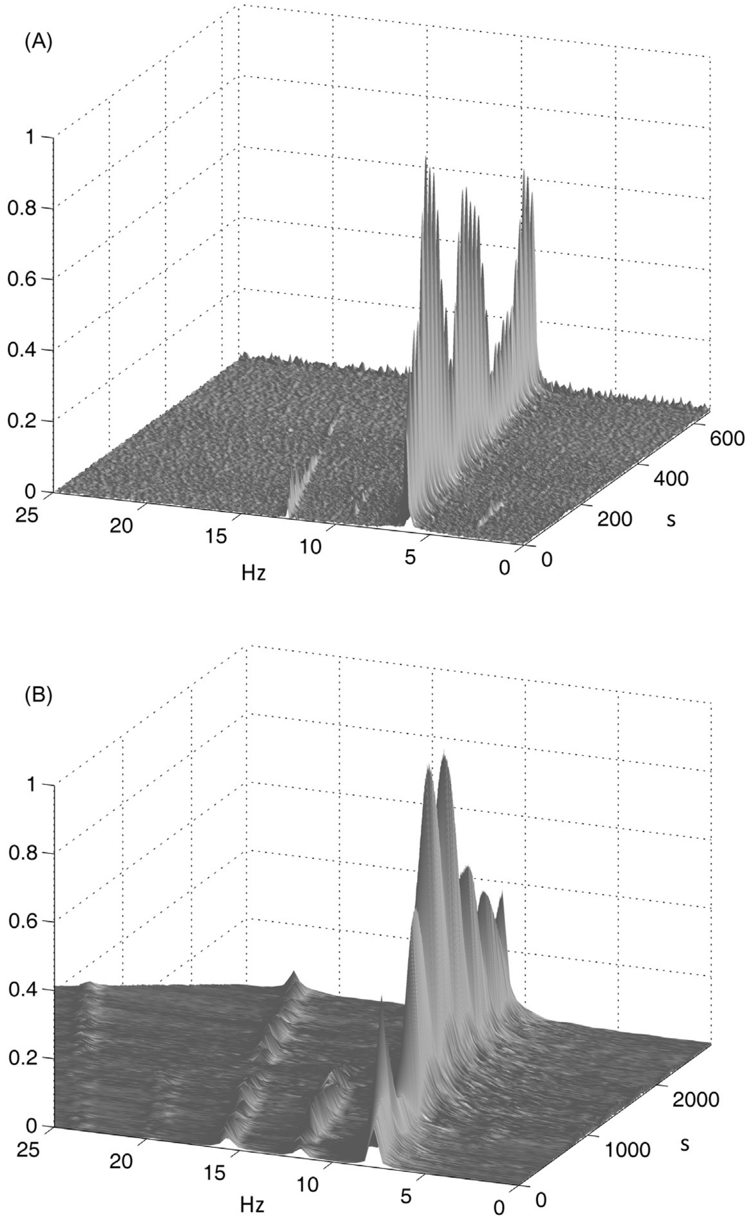

FIGURE 3.4.1

STF of oscillations with linear frequency modulation radiated by four types of vibrators: (A) the centrifugal vibrator CV-100 (in the main frequency range of 5.5–8.5 Hz); (B) the hydro-resonance vibrator HRV-50 (in the main frequency range of 5–7 Hz); (C) the centrifugal vibrator CV-40 (in the main frequency range of 6.25–9.57 Hz; (D) the hydraulic vibrator HV-10/100 (in the main frequency range of 10–60 Hz). Higher harmonics are clearly defined from all vibrators. In all cases the STFs correspond to records along the vertical component, *Z*. *STF*, Spectral-temporal functions.

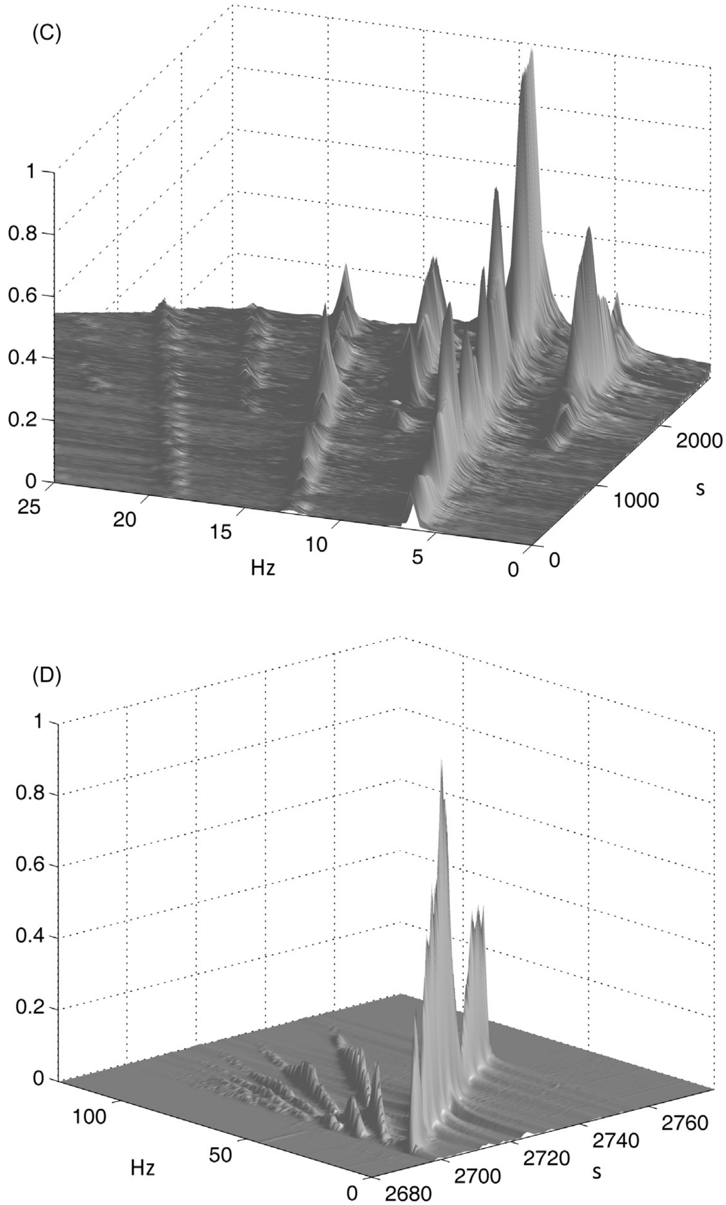

FIGURE 3.4.1

Continued

Below, we present the results of data analysis, taking into account the nonlinear effects of the seismic wave field. When the source conducts sweeps in a wide frequency band, the algorithm for calculating vibrational seismograms is based on the correlation convolution between the recorded seismic signals and the reference signal, which repeats the shape of the sounding signal from the oscillation source: $u(t_i)Nv(t_i)$, ($i = 1,\ldots,N$—the number of sample values of both types of signals). Here $u(t_j)$ is the recorded seismic signal, and symbol N means correlation convolution. The reference signal $v(t_i)$ has the form $v_1(t_i) = A\cos(\omega_0 t_i + \beta t_i^2/2)$ for the base frequencies and $v_2(t_i) = A\cos(2\omega_0 t_i + \beta t_i^2/2)$ for the second harmonics; coefficient β characterized the frequency sweep rate. In the case, when the signal $v_1(t_i)$ is within a 5.5−8.5 Hz frequency band, then $v_2(t_i)$ has an 11−17 Hz frequency band. We recorded vibrational seismograms corresponding to different distances from the vibrator, namely, 20 and 50 km (Fig. 3.4.2).

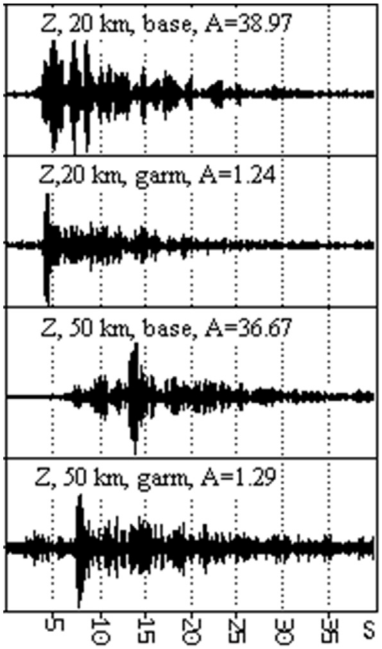

FIGURE 3.4.2

Vibrational seismograms for base (marked as "base") and second (marked as "garm") harmonics at distances of 20 and 50 km. The second harmonic constitutes about 3% at a distance of 20 km and about 17% at a distance of 50 km from the source (Z-component). These values are determined by the ratio of the amplitude maxima of the second and base seismograms. Greater contrast between the arrivals of primary waves in the second harmonic is observed.

In these figures, the amplitudes of dominant waves are additionally presented, in discrete units of the analog-to-digital converter. It is clear that seismograms of the second harmonics are characterized by the sharper arrivals of first (longitudinal) waves (4.9 seconds at 20 km, 7.8 seconds at 50 km), which increase the accuracy of measurement for wave arrival times. From the point of view of seismic physical processes, the higher contrast in the arrival of P-waves results from their saturation at the high frequencies of the second harmonics. The levels of nonlinear effects, determined by the ratio between the amplitude maxima of the secondary and base seismograms, are 3% and 17% respectively.

3.4.3 Nonlinear processing of vibrational seismograms

In deep vibroseismic sounding (DVS) of the Earth, there are some difficulties in determining the arrival times using vibrational seismograms obtained from a source located long distances away (hundreds of kilometers). The difficulty stems from the limited power and limited range of the vibrator excitation frequencies, compared to powerful explosions. Here, the influence of external noise on the process of wave detection is significant. Some authors (Glinsky et al., 2000) avoid these difficulties using synchronous stacking of vibrograms (vibrational seismograms) along the lineup axes and over a series of repeating sounding sessions. In their case, the dependence of the total wave amplitude on the direction of summation creates the effect of directional sensitivity, which, by analogy with antennas, can be called a directional characteristic. Attempting to increase the accuracy in determining the wave arrival time using a limited number of seismic receivers ($n \sim 5$) raises the notion of nonlinear processing, which forms the basis of the multiplicative antenna. In this case, in contrast to antennas with linear processing, we can achieve more accurate resolution in the direction of wave propagation with nonlinear processing, using the same number of antenna elements. In the case of n sensors, the output signal for nonlinear processing has the form:

$$u_M = \overline{u_1 \cdot u_2 \cdot \cdots \cdot u_n} \sim F_E{}^n \cdot \Psi_1(k, \eta, d) \tag{3.4.1}$$

Whereas, for linear processing, it has the form:

$$u_\Sigma = \overline{u_1 + u_2 + \cdots + u_n} \sim n \cdot F_E \cdot \Psi_2(k, \eta, d) \tag{3.4.2}$$

where F_E is the envelope of the seismogram at the output of one sensor; ψ_1, ψ_2 is the trigonometric functions of the parameters k, η, d, rapidly changing with respect to the envelope.

Here $k = 2\pi/\lambda$ is the wave number, η is the angle between the incoming wave front and perpendicular to the line of the seismic sensors locations; d is the distance between adjacent sensors, and n is the number of sensors. Amplitude variations of the functions Ψ_1 and Ψ_2 are limited, since they are formed from trigonometric functions. Taking this into account, functions F_E are determined in Eqs. (3.4.1) and (3.4.2).

The vibrational seismogram obtained as a result of intercorrelation convolution consists of waveforms characterized by symmetry with respect to the arrival times of the waves. Hence its arrival time is determined by the maximum of the wave amplitude. The variations in the wave arrival estimate in the direction of propagation η were determined by the second derivative (Tikhonov, 1983) in the form $D_\eta = -1/\left(d^2u(\eta)/d\eta^2\right)|_{\eta_0}$, where η_0 corresponds to the best sensitivity of the receivers achieved in the direction of wave front propagation. For a particular case, when $\eta_0 = 0$ (perpendicular wave front incidence) $F(\eta_0) = 1$, at $n \gg 1$ for nonlinear processing $D_{\eta 1}$ has the order $\sim 1/n^2$, and for linear processing has the order $D_{\eta 2} \sim 1/n$. Thus, the error in determining the wave propagation direction is for nonlinear processing [Eq. (3.4.1)] by a factor of n smaller than for linear processing [Eq. (3.4.2)]. The high resolution of nonlinear processing is illustrated for the vibrational seismograms obtained from the CV-100 vibrator at DVS in the Degelen−Bystrovka direction (Fig. 3.4.3).

The recording points were located at distances of 304, 342, and 371 km from the vibrator CV-100. The sounding was made by sweep-signals in the 5.85−8.0 Hz frequency range, with a frequency sweep duration of 31 minutes, 29 seconds.

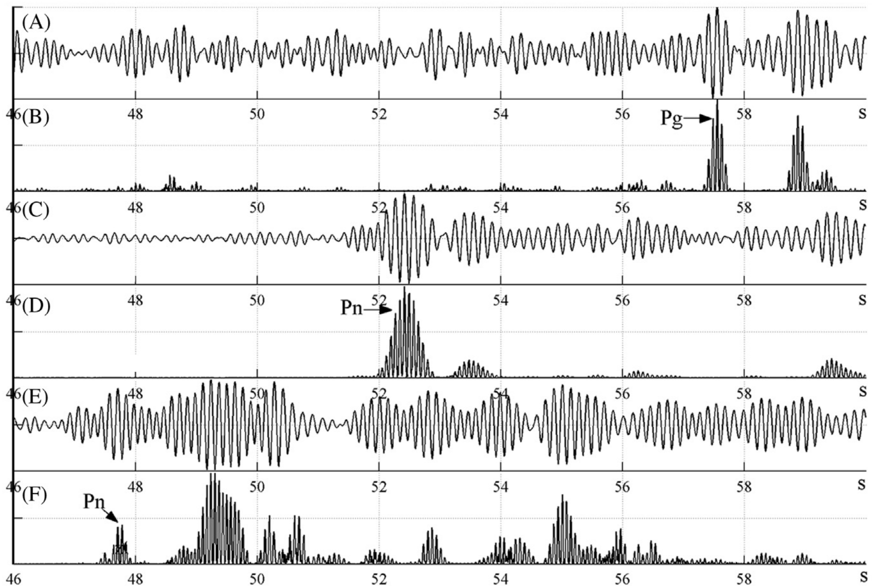

FIGURE 3.4.3

(A, B, C) Seismograms with linear processing; (D, E, F) seismograms with nonlinear processing. Nonlinear processing produces more distinguishable arrivals of primary waves and a higher accuracy in determining their arrival times.

The top of Fig. 3.4.3 contains seismograms at (A)—371 km, (B)—342 km, and (C)—304 km, obtained by linear summation of $n = 5$ seismic traces along theoretical travel-times (hodographs) corresponding to the waves refracted from the Moho boundary ($V_p = 8.1$ km/s). In Fig. 3.4.3 (bottom), the seismograms are for: (D)—371 km, (E)—342 km, and (F)—304 km, obtained by nonlinear processing of the same data as for linear processing. Comparing the results of both types of processing shows that after the nonlinear processing, the contrast in P_n-wave arrivals and the sharpness of their maxima are greater than after the linear processing. For these distances, the arrival times of compressional waves P_n are 56, 52.5, and 47.6 seconds, respectively.

3.4.4 Nonlinear phenomena in seismic monitoring

Modern concepts of earthquake source development, based on the kinetic theory of rock failure by Zhurkov (1968) and the multidisciplinary approach by Alekseev et al. (1998), consider the processes of intensive fracturing involved in potential earthquake zones. Following their approach, we use crack density function θ (x, y, z, t) for spatial coordinates and time to characterize the medium.

For seismic methods, we use the parameters (such as amplitude, frequency, and phase) of observed longitudinal and transverse waves to obtain more detailed information about the changes in fractured zones. Alekseev et al. (2004) suggest that the dynamic characteristics of the wave field are most sensitive to changes in the geological medium's elasticity. Also, the medium's fracturing is a likely physical basis for development of the seismic event. This suggests that the nonlinear components (such as multiple harmonics) in the recorded wave fields should be taken into account (Glinsky et al., 2006). Thus, it is important to find the relationship between the wave field nonlinearity and the parameters of a medium's fracturing.

Such a relationship was obtained by Verbitsky (1987) for a model of a fractured zone in a homogeneous isotropic medium with the elasticity modulii K_1, μ_1 and density ρ_1. Uniformly scattered and randomly oriented spheroidal voids were taken as the initial model of fracturing. The shape of the voids is determined by the parameter α, which is equal to the ratio between the rotation axis length of a spheroid and the length of its second axis. The distribution of the relative volume of voids between its minimal value $\alpha_{\min}$ and maximal value $\alpha_{\max}$ is described by the function $\varphi(\alpha)$. It is assumed that the length of an elastic wave with the highest frequency propagating in the medium being modeled is much greater than the linear dimensions of the largest voids.

The following relationships are used for the effective elasticity module of a medium with spheroidal voids (Verbitsky, 1987):

$$K_{(1)} \approx K_0 \left[1 - \varphi_{real} a \frac{K_0{}^2}{p_0 K_1} f(\alpha_0) u_{ll} \right],$$

$$\mu_{(1)} \approx \mu_0\left[1 - \varphi_{real} b \frac{K_0\mu_0}{p_0\mu_1} f(\alpha_0) u_{ll}\right],$$

Here $K_0 \approx K_1\left(1+\varphi_{real} aF\right)^{-1}$, $\mu_0 \approx \mu_1\left(1+\varphi_{real} bF\right)^{-1}$,
$a = \left(\left(4\left(1-\nu_1^2\right)\right)/(3\pi(1-2\nu_1))\right)$, $\quad b = \left((8(1-\nu_1)\cdot(5-\nu_1))/(15\pi(2-\nu_1))\right)$, $f(\alpha_0) = \left((\varphi(\alpha))/\varphi_{om}\right)$,

$\varphi_{real} = \int_{\alpha_0}^{\alpha_{\max}} \varphi(\alpha)\, d\alpha$ is the initial value of the medium's fracture porosity; $F = \int_{\alpha_0}^{\alpha_{\max}} f(\alpha)/\alpha\, d\alpha$; ν_1 is Poisson's coefficient, K_0 is the effective compression modulus of the microfractured medium, and u_{ll} is the sum of diagonal components of the dynamic deformation tensor.

The equation of propagation for plane monochromatic elastic waves along the OX-axis in the medium being modeled when only longitudinal motions are present in this medium ($u_x \neq 0,\ u_z = u_y = 0$) has the form:

$$\rho_0 \frac{\partial^2 u_x}{\partial t^2} - M_0 \frac{\partial^2 u_x}{\partial x^2} = B \frac{\partial u_x}{\partial x} \cdot \frac{\partial^2 u_x}{\partial x^2} \tag{3.4.3}$$

At the boundary condition $u_x(0,t) = U_x \sin \omega\, t$, the solution to the equation in a second approximation has the following form (Verbitsky, 1987):

$$u_x = U_x \sin \omega \left(t \mp \frac{x}{c_P}\right) - \left(\frac{U_x}{2}\right)^2 \frac{B}{M_0} {k_P}^2 x \cos 2(\omega\, t \mp k_P x), \tag{3.4.4}$$

where $\quad k_P = \omega/c_P, \quad B = -3\varphi_{\text{real}}\left(K_0/p_0\right)\left(a\left({K_0}^2/K_1\right) + \left(4/3\right) b\left({\mu_0}^2/\mu_1\right)\right) f(\alpha_0)$, $M_0 = K_0 + \left(4/3\right)\mu_0$, x is wave travel length.

It follows from Eq. (3.4.4) that in a fractured medium, there appears a harmonic with doubled frequency. The harmonic's amplitude is determined by the coefficient B, which depends on the medium's fracturing parameters, the Mach number $M = U_x\omega/c_P$, and the wave travel length Jt, increasing proportionally with x. This phenomenon was noted earlier as an accumulating nonlinearity in a nonlinearly elastic medium (Polyakova, 1964). Taking into account Eq. (3.4.4), the coefficient of nonlinearity for the monochromatic wave is determined by the ratio between the amplitudes of the fundamental and second harmonics:

$$\frac{u_2}{u_1} = \frac{1}{8} \frac{U_x B {k_P}^2 x}{M_0} \tag{3.4.5}$$

Eq. (3.4.5) relates the parameters of wave-field nonlinearity to the medium's fracturing (determined by the parameter B), which depends on the sizes of fractures and their distribution density, as well as on the medium's elasticity modulus. Taking into account this dependence and the aforementioned role of fractures in earthquake development, it is likely that the dynamic parameters of wave-field nonlinearity can be successfully used as an important parameter for monitoring.

We analyzed the nonlinearity coefficient from Eq. (3.4.5) as a function of the medium's fracturing, the amplitude of particle velocity U_x, and the distance x. Water-saturated fractured granite was chosen as the medium, with the following elasticity parameters: Young's modulus $E = 2.216 \cdot 10^9$ Pa, Poisson's coefficient $\nu = 0.44296$, static pressure $p_0 = 10^3$ Pa, frequency $f = 10$ Hz, and propagation velocity of the P-wave in granite $C_p = 5000$ m/s. The curves in Fig. 3.4.6 show the nonlinearity coefficient of the monochromatic wave for these parameters versus the ratio between the ellipsoid axes describing an elementary fracture. Curves 1 and 2 were computed for the wave propagation length $x = 10$ km; curves 3 and 4 for 100 km. The medium's particle velocity $U_x = 2.7 \times 10^{-8}$ m/s corresponds to curves 1 and 3, the velocity of 70×10^{-8} m/s corresponds to curves 2 and 4.

The presence of maxima in the plots indicates that the nonlinear effects of wave propagation predominate in inhomogeneous media with limited sizes of inhomogeneities.

The dependence of the second harmonic's amplitude on the propagation distance in an attenuating medium can be described by the following relationship (Zarembo and Krasilnikov, 1966):

$$a_2 = \frac{K_c x \omega^2 a_1^2}{8 c_{p,s}^2} \tag{3.4.6}$$

Here, x is the wave travel length, K_c is the nonlinearity coefficient of the medium determined by the expression $K_c \approx \rho\nu\left(\triangle\nu/\triangle p\right) \approx \left(\triangle\nu/\nu\right)\triangle\theta$, in which ρ is the density, $\Delta\theta$ is the volume deformation variation, Δp is the pressure variation, a_1 is the amplitude of the first harmonic, and $c_{p,s}$ is the velocity of the P- or S-wave. The value of this coefficient estimated by some authors is $K_c \approx 10^3$. As an illustration, Fig. 3.4.5 presents curves for the nonlinear effect "accumulation" versus distance at given seismic velocities, in a "source−receiver" distance range of 0.3−355 km. Curves correspond to the velocity $C_p = 5500$ m/s and to the velocity $C_s = 3500$ m/s. The nonlinearity coefficient is obviously larger for smaller seismic velocities.

It follows from an analysis of Figs. 3.4.4 and 3.4.5 that the ratio between the second and the base harmonics can increase by several times as the wave travel path increases. The presence of maxima in the plots (Fig. 3.4.4) indicates that the nonlinear effects of wave propagation predominate in inhomogeneous fractured media.

The nonlinearity parameters of the wave field at large distances also carry the influence of the vibrator nonlinearity (Glinsky et al., 2002). Changes in the initial ratios between the second and fundamental harmonics a_{02}/a_{01} vary (depending on the distance) in accordance with the following approximate law, which is valid for long observation distances (hundreds or more kilometers) and low frequencies:

$$\frac{a_{f_2}(x)}{a_{f_1}(x)} = \frac{a_{02}}{a_{01}} \exp[(\alpha_2 - \alpha_1)(x - x_0)] \tag{3.4.7}$$

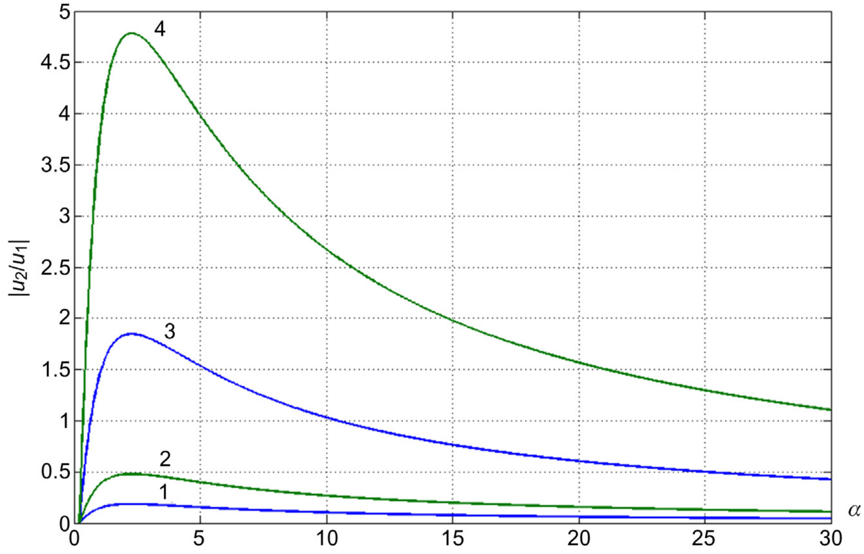

FIGURE 3.4.4

The ratio between the second and base harmonics versus the geometrical parameters of the medium's inhomogeneity due to fracturing. Young's modulus $E = 2.216 \times 10^9$ Pa, Poisson's coefficient $\upsilon = 0.44296$, static pressure $P_0 = 10^3$ Pa, frequency $f = 10$ Hz, propagation velocity of the P-wave in granite $C_p = 5000$ m/s. Wave travel path: $x = 10$ km for curves 1 and 2, and $x = 100$ km for curves 3 and 4. Oscillating speed $U_x = 2.7 \times 10^{-8}$ m/s for curves 1 and 3; $U_x = 70 \times 10^{-8}$ m/s for curves 2 and 4. The presence of maxima in the plots probably indicates that nonlinear effects of wave propagation predominate in inhomogeneous media with limited linear sizes of inhomogeneities.

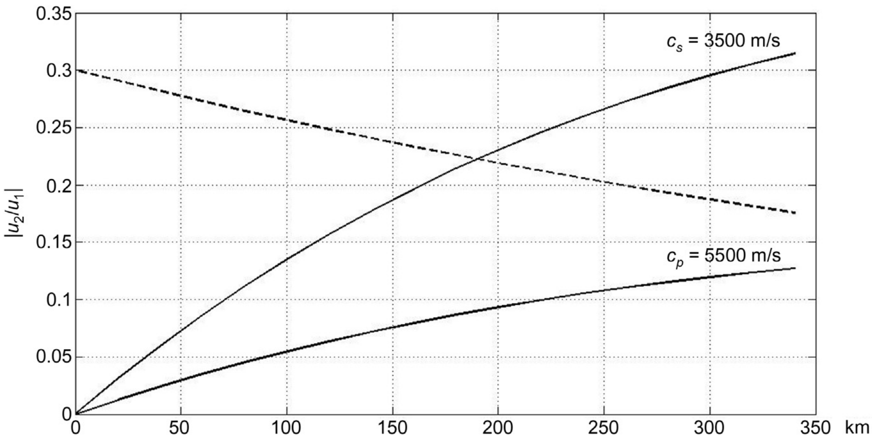

FIGURE 3.4.5

Coefficient of nonlinear distortions versus distance at different seismic velocities: $C_p = 5500$ m/s, $C_s = 3500$ m/s. Attenuation of this coefficient due to wave energy absorption in the medium is shown by a dashed line. The data are for the radiation regime of harmonic oscillations at a basic frequency of 6.3 Hz.

where $\alpha_{1,2} \approx 2.5 \cdot 10^{-4} f_{1,2}$ $(1/км)$ is the medium's attenuation coefficient, and x_0 is the "source−receiver" distance near the nonlinear volume center.

As an example, the dashed line in Fig. 3.4.5 shows the attenuation curve [Eq. (3.4.7)] for the cases in which $f_1 = 6.3$ Hz and $f_2 = 12.6$ Hz. Therefore, the effect of propagation distance on nonlinear parameters is driven by a resonance linear increase [Eq. (3.4.6)] and by an exponential decrease due to attenuation [Eq. (3.4.7)]. The combined effect of these two factors defines the natural spatial bounds of the nonlinear effect.

3.4.5 Experimental results

The nonlinearity effect was estimated using monochromatic signals, based on the amplitude ratios of the second and base harmonics. The spectrograms for the sums of monochromatic signals and noise confirm the possibility of detecting both types of harmonics at a "source−receiver" distance of 355 km—in this case, the signal of the base harmonic had a frequency of 6.3 Hz, whereas the frequency of the second harmonic was 12.6 Hz (as presented in Fig. 3.4.6A and B, respectively). The parameters of the spectrograms are shown in the upper part of the figures: m is the amplitude of the spectral peak at the frequency f, and ρ is the ratio between the amplitude m and the root-mean-square value of noise. It follows from the spectrograms that this ratio for both signals is 0.48. At the same time, the calculated [using Eq. (3.4.7)] ratio at this distance and frequency is 0.14. We attribute this difference to the contribution toward the propagation nonlinearity originating in the medium.

It seems proper to take into account the information coming from higher harmonics in seismically active zones, as well as in studying geodynamic processes. We illustrate this below by monitoring changes in the Earth's crust during lunar−solar tides. The amplitude ratios for the second and base harmonics were recorded during periodically repeating (over a 3-hour period) sounding sessions using mono-frequencies generated by a powerful CV-100 seismic vibrator. Each session consisted of sequentially radiated 20-minute-long oscillations at frequencies of 6.3 and 7.0 Hz. These sessions were continuously repeated over a 4-day period.

The main objective of the experiment is described in detail in Glinsky et al. (2000). This paper investigates the possibility of selecting daily and half-daily periodicities for varying the parameters of the seismic field for lunar−solar tides. We recorded all three (X, Y, and Z) components. The plots in Fig. 3.4.7 reflect the ratios between the second and the base harmonics at frequencies of 6.3 and 7 Hz. These data correspond to the parameters of the radiated seismic field in immediate proximity to the source (at a distance of 30 m). It is clear that the greatest

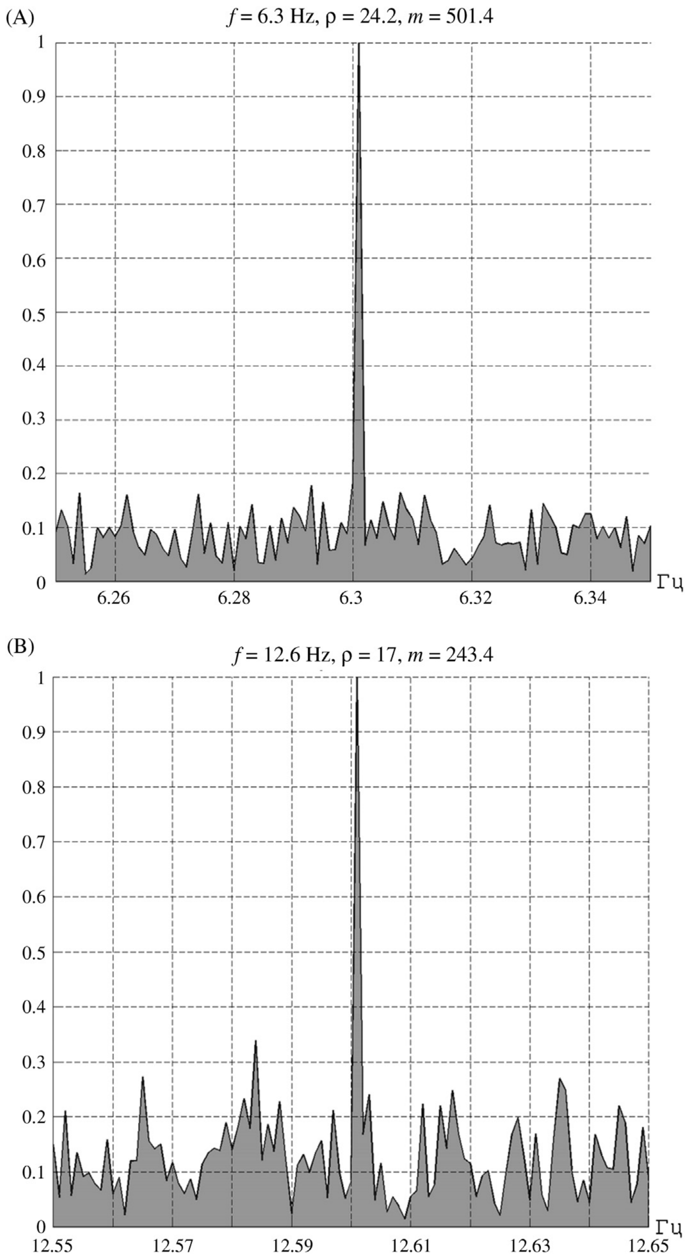

FIGURE 3.4.6

Spectrograms of the base (A) and second (B) harmonics at a distance of 355 km. Here f is the basic frequency radiated by the source, ρ is the signal/noise ratio, and m is the amplitude of the harmonic.

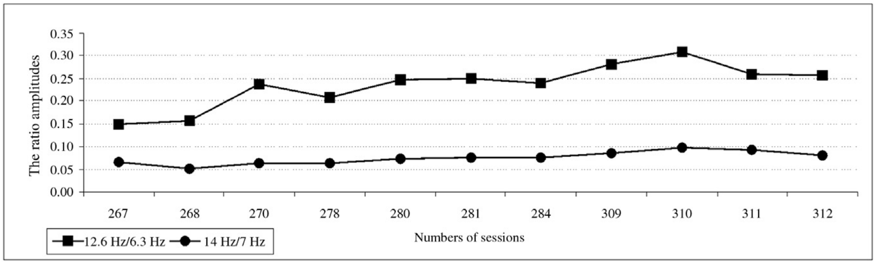

FIGURE 3.4.7

Ratio between the second and base harmonics at the source. Sessions: 267–312.

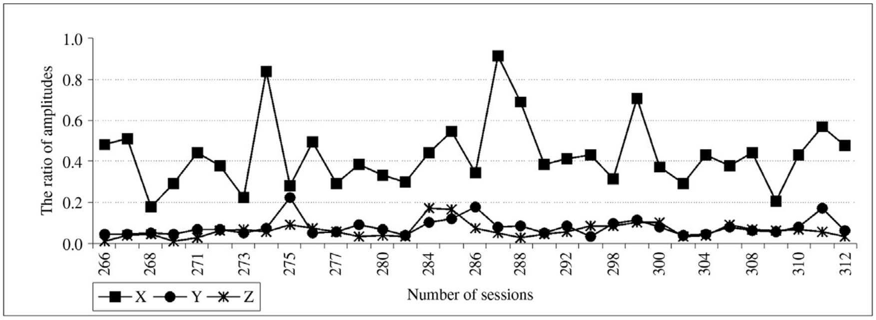

FIGURE 3.4.8

Ratio between the second (12.6 Hz) and base (6.3 Hz) harmonics at the 5th gauge. Sessions: 266–312.

nonlinear effect manifests itself at a frequency of 6.3 Hz. Here, the ratio of harmonics varies within 15%–30%; at the frequency of 7.0 Hz, this ratio is within 5%–10%.

Fig. 3.4.8 shows similar ratios obtained at a distance of 355 km from the source, corresponding to the components *X*, *Y*, and *Z*, and the source frequency of 6.3 Hz. These data show that the largest values of the ratios are at component *X* oriented to the vibrator. The ratios of harmonics at the considered distance are, on average, higher than those observed near the source. In particular, we have 50% against 25% at 6.3 Hz. External noise causes fluctuations in the obtained ratios (from session to session).

We relate the observed increase in the nonlinear component at long observational distances to the contribution of propagation nonlinear effects. It follows from this assumption that changes in deformation-related nonlinear effects caused by lunar–solar tides can be detectable. It is known (Melchior, 1966) that many geophysical fields are characterized by daily and half-daily periodicity. Latent periodicity in the series was selected with the use of the discrete

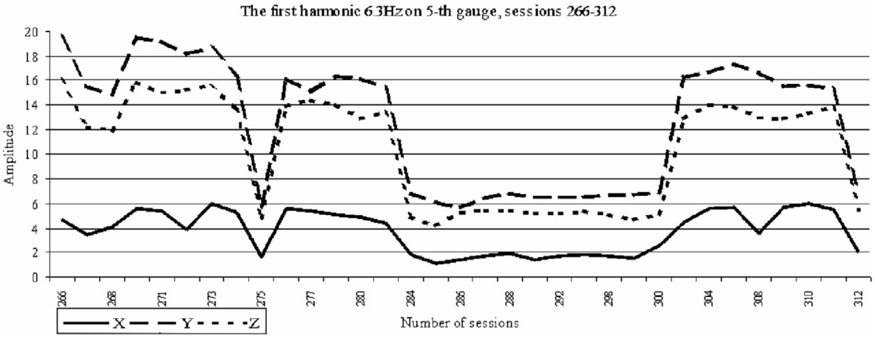

FIGURE 3.4.9

Levels of radiated signals in the source zone.

Fourier transform, employing the weight function to smooth the edges of the observation series.

The graphs representing the amplitudes of the base harmonics close to the source depending on the session number [at a frequency of 6.3 Hz and the components *X*—(solid line), *Y*—(dotted line), *Z*—(dashed line)], are presented in Fig. 3.4.9. This figure shows that some of the sounding sessions had sharp decreases in amplitude levels, caused by an "artificial" decrease in the power of the original CV-100 vibrator. Despite this, the stability in detecting half-daily and daily periodicities resulting from the lunar tides, at the remote recording point, was retained. However, the above periodicities are not visible in the amplitude graphs for just the base harmonic at a frequency of 6.3 Hz. The likely reason for this is that the fluctuations in the radiation oscillation levels bring about corresponding fluctuations in the signal levels at the receiving point. At the same time, when the harmonic ratio is used, the correspondent fluctuations cancel (Fig. 3.4.7), and it becomes possible to detect daily and half-daily periodicities.

Fig. 3.4.10 shows the results from this selection for the observation series corresponding to the ratios between the amplitudes of the second and base harmonics with sounding frequency 6.3 Hz (curve II). The curve represents the observation series corresponding to component *Z*. For comparison, the plot shows the amplitude spectrum of gravitational variations recorded for the same period (curve I). It follows that daily periodicity is confidently distinguished within the time series $a_{12.6}(355)/a_{6.3}(355)$. Half-daily periodicity is expressed weakly.

One advantage of the monitoring method proposed here is its stability with respect to fluctuations in the amplitude of radiated waves, owing to the seasonal and instrumental variations. This was confirmed experimentally from the comparative analysis of the test recordings near the source, and of the ratios between the amplitudes of secondary and fundamental waves at a distance of 355 km.

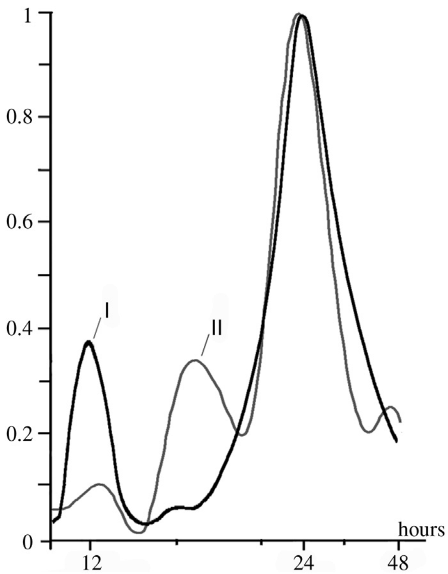

FIGURE 3.4.10

Amplitude spectrum of time variations caused by Earth tides: curve I: gravity variations, curve II: variations of relations between second and base harmonics for during the monitoring of a 355-km-long Earth's crust zone with a sounding frequency of 6.3 Hz.

3.4.6 Discussion

Active seismic monitoring with the use of powerful seismic vibrators is accompanied by nonlinear wave effects developing during both the radiation and propagation of seismic waves. These effects occur because of imperfections in the source−ground coupling, as well as because of the soil nonlinearity under the vibrator. Nonlinear wave-propagation effects occur in soil and rocks, which attenuate seismic waves. Accounting for both nonlinearity and attenuation contributes to an increase in the accuracy and sensitivity of active monitoring technology, mostly as a result of the following factors:

- Seismograms of the second harmonic are characterized by sharp arrivals of the first (P-) waves, which increase the accuracy of measurement for the arrival times of waves and their time resolution. The sharpness of the P-wave arrivals is caused by the high frequencies of the second harmonics. Additional use of the frequency band of second harmonics further saturates the spectrum of P-waves with higher frequencies, which contributes to an increase in the contrast of wave arrivals. This is confirmed by detection and measurement of the arrival times of P-waves at distances up to 50 km (Fig. 3.4.2).

- Nonlinear radiation effects are associated with the choice of the sounding regime: They are maximal in the harmonic regime, when the second harmonics can reach 50% and more from level the basic harmonics (Fig. 3.4.6). It is shown especially at near-resonant frequencies during a long sounding.

  In the regime of sounding by wideband signals (sweeps), these phenomena are less pronounced, since they do not have enough time to fully develop because of frequency scanning. Quantitatively, within the broadband sounding regime, the nonlinear effects do not exceed 10%. Given this fact, the phenomenon of radiation nonlinearity can be more effectively used in the harmonic regime of sounding.
- Low-frequency vibrators are characterized by a limited effective frequency band of sounding signals. The ratio between the upper and lower frequencies of the frequency band is about 1.5−1.8. This is the reason for the lower contrast in the arrivals of the main wave types and their visibility on the noise background. Our successful attempt to increase the accuracy in determining the wave arrival time within seismograms, obtained for a limited frequency range at basic frequencies and at a limited number of seismic receivers ($n = 5$), raises the possibility of using the principle of nonlinear processing. It forms the basis of the multiplicative antenna. In this case, in contrast to antennas with linear processing, one can achieve more accurate resolution in the direction of wave propagation with the same number of antenna elements.
- In conducting active vibroseismic monitoring, we must account for the influence of seasonal and instrumental variations in the parameters of the radiation field, since they limit the sensitivity of the vibroseismic method. To eliminate source-related variations, we have proposed a statistical algorithm for processing observational data, based on the measurement of the amplitudes for the second and base harmonics at the background of noise and the calculation of their ratios. The stability of the algorithm from the variations in the force characteristics of radiation, and its high sensitivity to variations in the medium's rigidity parameters caused by geodynamic processes, are proved by detection of daily and half-daily periodicities. These were obtained from seismic-observation data from the periods of the Earth's tides at a source−receiver distance of 355 km. The obtained results correlate well with the results from processing of the gravimetric observation data.
- Taking into account the above, we find it very likely that high harmonics carry useful information; information that can help in monitoring geodynamic processes in seismically active zones.

3.4.7 Conclusion

In this work, we have studied the problem of increasing the informational content from the processing of seismic monitoring data, taking into account the nonlinear effects of wave fields at the stages of radiation and propagation of seismic oscillations in elastic media. We estimated the quantitative nonlinear characteristics related to the radiation and propagation of seismic wave fields generated by powerful ground-based vibrators. We developed a statistical algorithm for the processing of recorded seismic data, based on the amplitude ratios of the second and base harmonics. We found that the proposed algorithm is robust, even when variations in the source are present, and that it is sensitive to variations caused by geodynamic processes. This is especially important for long-term monitoring of the processes occurring in seismic-prone regions.

Acknowledgments

This research was supported by the Russian Foundation for Basic Research, Grants No. 17-07-00872-a, 16-07-01052, and 18-47540006 p_a.

The authors thank Dr. Nitoshi Mikada for careful reading of the manuscript and comments made.

References

Alekseev, A.S., Geza, N.I., Glinsky, B.M., Emanov, A.E., Kashun, V.N., Kovalevsky, V.V., et al., 2004. Active Seismology with Powerful Vibrosources. ICM&MG SB RAS, Filial Geo Publishing House of the SB RAS, Novosibirsk (in Russian).

Alekseev, A.S., Belonosov, A.S., Petrenko, V.E., 1998. Determination of an integral earthquake precursor with the use of a multidisciplinary – model and active vibroseismic monitoring. Bull. Novosibirsk Comput. Center, Ser.: Math. Model. Geophys. 7, 3–36.

Brekhovskich, L.M., Goncharov, W.A.V., 1982. Introduction to a Mechanics of the Continuous Medium. Nauka, Moscow (in Russian).

Glinsky, B.M., Khairetdinov, M.S., Sedukhina, G.F., 2006. Geophysical data processing with tor nonlinear effects of radiation and propagation of elastic waves. Optoelectron., Instrum. Data Process. 42 (5), 37–44.

Glinsky, B.M., Khairetdinov, M.S., Kovalevsky, V.V., 2002. Nonlinear wave effects in the powerful seismic vibrators zone. In: Nonlinear Acoustics at the Beginning of the 21st Century, vol. 1. pp. 327–330.

Glinsky, B.M., Kovalevsky, V.V., Khairetdinov, M.S., 2000. Vibroseismic monitoring of earthquake prone areas. Volcanol. Seismol. 21, 723–730.

Korneev, V.A., Nihei, K.T., Myer, L.R., 1998. Nonlinear Interaction of Plane Elastic Waves: Scientific Report, LBNL-41914. Lawrence Berkeley National Laboratory, Berkeley, CA, 94720.

Melchior, P., 1966. The Earth Tides. Pergamon Press, New York.

Nikolaev, A.V., 1987. Problems of nonlinear seismics. Collection of Articles Problems of Nonlinear Seismics. Nauka, Moscow', pp. 5–20.

Rudenko, O.V., Soluyan, S.I., 1975. Theoretical Fundamentals of Nonlinear Acoustics. Nauka, Moscow' (in Russian).

Polyakova, A.L., 1964. Nonlinear effects in a solid. Sov. Phys., Solid State 6 (1), 50–54.

Tikhonov, V.I., 1983. Optimal Signal Reception. Radio I Svyaz', Moscow (in Russian).
Verbitsky, T.Z., 1987. Peculiarities of elastic wave propagation in nonlinearty elastic porous media. Problems of Nonlinear Seismics. Nauka, Moscow, pp. 94–103.
Zarembo, L.K., Krasilnikov, W.A., 1966. Introduction to Nonlinear Acoustics. Nauka, Moscow (in Russian).
Zhurkov, S.N., 1968. Kinetic concept of strength of solid bodies. Vesmik Akademii. Nauk SSSR 3, 46–52.

Further reading

Alekseev, A.S., Chichinin, I.S., Korneev, V.A., 2005. Powerful low-frequency vibrators for active seismology. Bull. Seismol. Soc. Am. 95, 1–17.
Khairetdinov, M.S., 2003. The nonlinear wave effects in vibroseismic. Bull. Novosibirsk Comput. Center, Ser.: Math. Model. Geophys. 8, 59–68.